UCRL-JRNL-218647

LAWRENCE
LIVERMORE
NATIONAL
LABORATORY

# New Dust Belts of Uranus: One Ring, Two Ring, Red Ring, Blue Ring

I. de Pater, H. B. Hammel, S. G. Gibbard, M. R. Showalter

February 3, 2006

Science

# New Dust Belts of Uranus:

# One Ring, Two Ring,

# Red Ring, Blue Ring


Imke de Pater

Astronomy Department, 601 Campbell Hall

University of California, Berkeley, CA 94720

imke@astron.berkeley.edu

Heidi B. Hammel

Space Science Institute

4750 Walnut Street, Suite 205, Boulder, CO 80301

Seran G. Gibbard

Lawrence Livermore National Laboratory

Livermore, CA 94550 USA

Mark R. Showalter

SETI Institute

515 North Whisman Road

Mountain View, CA 94043



Submitted to *Science*: January 17, 2006

## ABSTRACT

We compare near-infrared observations of the recently discovered outer rings of Uranus with HST results. We find that the inner ring, R/2003 U 2, is red, whereas the outer ring, R/2003 U 1, is very blue. Blue is an unusual color for rings; Saturn's enigmatic E ring is the only other known example. By analogy to the E ring, R/2003 U 1 is probably produced via impacts into the embedded moon Mab, which apparently orbits at a location where non-gravitational perturbations favor the survival and spreading of sub-micron sized dust. R/2003 U 2 more closely resembles Saturn's G ring.

Showalter and Lissauer *(1)* reported the detection of two faint rings, R/2003 U 1 (henceforth "R1") and R/2003 U 2 (henceforth "R2"), located well outside Uranus' main ring system. R1, the outer ring, is centered on the orbit of the tiny moon Mab, whereas R2 orbits between moons Rosalind and Portia but has no visible source bodies. Using the Keck adaptive optics system at near-infrared wavelengths, we show that R2 is red, while R1 is extremely blue. The colors, location, and radial extent of the two rings, as well as the association of ring R1 with moon Mab, make the uranian system in many ways remarkably similar to Saturn's outer ring system.

We imaged Uranus and its ring/moon system with the near-infrared camera NIRC2, coupled to the adaptive optics system, at the W. M. Keck II telescope on UT 23 August and 28 October, 2005. We observed in the K' band (2.2 μm), where sunlight is absorbed by methane and hydrogen gas in Uranus's atmosphere, greatly reducing scattered light from the planet. The ring opening angle, *B*, was 8.4° in August and 10.5° in October. The pixel size was ~ 140 km (0.01″) and the effective resolution ~ 650 km. The full field of view was 10″ or 140,000 km. All images were processed using standard techniques *(2, 3)*. The intensities were converted into units of *I/F*, a dimensionless quantity, where *I* is the observed intensity and π*F* is the solar flux density received by Uranus at K'.

The total integration time on 23 August was 1 hour. R2 was readily detected on the planet's south side (Fig. 1A), but only the ring's tip could be seen in the north, near the edge of the frame. Both ring ansas fell at a radial distance of 67,350 ± 100 km, consistent with HST results *(1)*. In October we mosaicked images to cover a larger field (~ 25″) to search for R1. The total integration time across the image varies from 48 min up to 1.5 hours. We detected a portion of R2, but saw no trace of the outer ring R1, despite a very clear view of the system's ansas (Fig. 1B).

We averaged in longitude the visible parts of ring R2 to produce radial profiles (Fig. 2). These were then fit with a model *(2)* consisting of a uniform band of material that, after convolution with the point spread function (PSF), best matched the data. From the radial profiles we derive an "equivalent width" *EW*, defined as the radial integral of *I/F*. For an optically thin ring, *EW* varies in inverse proportion to $\mu \equiv \sin B$; hence, the "normal equivalent width" $\mu EW$, equal to what would be measured from a viewpoint normal to the ring plane, is better suited for comparisons. Our measurements of R2 from August and October are consistent after allowing for $\mu$, so we adopt their weighted average: $\mu EW = 1.30 \pm 0.13$ m *(3)*.

To increase our sensitivity to R1, we flipped the image (Fig. 1B) vertically and then averaged both images. A radial profile was extracted after averaging the data in longitude, but it shows no trace of the ring. Because R1 is quite broad at ~ 17,000 km *(1)*, the limiting factor in its detection is not the intrinsic noise in the data, but rather the more systematic uncertainty in the image background. Although this is difficult to quantify, we believe that a ring with $\mu EW = 1$ m might have just marginally escaped detection. We therefore adopt a generous upper limit of $\mu EW = 2.5$ m for R1 *(3)*.

Both rings were discovered in Hubble Space Telescope (HST) images through the clear filter (0.3–0.7 μm) of the Advanced Camera for Surveys (ACS). Our corresponding measurements from that data set are $\mu EW = 6.46 \pm 0.60$ m for R1 and $\mu EW = 0.63 \pm 0.09$ m for R2. The comparison between the visual and the infrared is striking: R2 is distinctly red whereas R1 is distinctly blue (Fig. 3).

Showalter and Lissauer *(1)* also detected the rings in forward-scattered visual light (phase angle $\alpha = 146°$) in the Voyager images. Using their measurements, we derive the high-phase to low-phase ratio *H* to be $4.2 \pm 0.5$ for R1 and $1.6 \pm 0.5$ for R2. Both rings are predominantly forward-scattering, with $H > 1$. This implies that both rings are very dusty, with particles predominantly in the sub-μm to μm size range. Such tiny grains cannot survive for long in planetary orbit, because they are subject to a variety of removal and destruction mechanisms *(4)*. Continuous replenishment from larger source bodies is required.

Typical dusty rings, such as Jupiter's ring system and Saturn's G ring, are red. The main rings of Uranus, where particle sizes of ~ 10 cm to 10 m dominate *(5)*, are essentially neutral in color *(6, 7)*. However, when dust is smaller than or comparable to the wavelength of light, the reflected color is dominated by particles size effects rather than the intrinsic color of the material. For a very steep size distribution dominated by the tiniest dust grains, blue light is reflected. For flatter distributions dominated by the larger grains, the color is red. Saturn's E ring is the only ring known to be blue *(8, 9)*. In Fig. 3 we compare the spectra of rings R1 and R2 with Saturn's distant and dusty E and G rings. The similarities in spectral slopes between the pairs of rings is striking.

Saturn's G ring and Uranus's R2 show many additional similarities. Both have no known source bodies. Both orbit at similar distances from the planet (Fig. 4): the G ring at 2.78 Saturn radii ($R_S$) and R2 at 2.64 Uranus radii ($R_U$). Both have triangular profiles, with a peak displaced inward from the middle of the ring. Both the HST and Keck detections of R2 show evidence for brightness variations with longitude, and Cassini images have recently revealed arcs in the G ring *(10)*.

The values in Fig. 3B have not been re-scaled; the rings are essentially equal in $\mu EW$. The rings are also similar in their forward-scattering nature, although uncertainties are large: $H = 2.6 \pm 1.0$ for the G ring in Voyager data *(11)*, compared to $1.6 \pm 0.5$ for R2. However, the available pre-Cassini data are inadequate to constrain the G ring's size distribution uniquely *(12)*.

All of these similarities suggest that comparable physical processes are at work in the two rings. The Pioneer 11 spacecraft detected the absorption signature of high-energy protons while passing over the G ring. Dust grains cannot absorb such energetic particles; a population of macroscopic bodies, cm-sized or larger, must be embedded within the ring *(8)*. Collisions between and/or meteoroid impacts into these bodies probably create the G ring. A similar process likely leads to the formation of R2. Perhaps the variations in longitude can be understood as the result of the occasional, large impact that injects an usual amount of dust into the ring.

The blue colors of Saturn's E ring and Uranus's R1 also invite comparison. Perhaps coincidentally, both rings again fall at similar distances from their planets (Fig. 4): 3.95 $R_S$ and 3.82 $R_U$. Both of these rings peak in *I/F* near the orbit of a single moon, Enceladus in the case of the E ring and Mab in the case of R1. Both show very broad and again triangular profiles, although the E ring is substantially larger in radial extent. The ring colors are more difficult to compare, because the Keck measurement of R1 is merely an upper limit. Also the rings are not similar in their high-low phase ratios: *H* ~ 17 for the E ring *(8)* but ~ 4 for R1.

Further studies by Cassini have not revealed any additional moons in the orbit of Enceladus; it appears likely that this moon is the sole source of the ring. This is supported by very recent images of dust streaming off the moon's surface *(13)*, which likely serves as the "fountain" of the E ring. Mab is 20 times smaller in radius and unlikely to be geologically active; R1's dust is therefore probably generated via the more conventional mechanism of ejecta from meteoroid impacts.

Given that R1 and R2 probably have such similar origins, why are their colors so different? Dynamical simulations of the E ring provide a clue *(4, 14, 15)*. Although the details vary, studies show that dust grains leaving Enceladus are distributed radially and vertically by a combination of Saturn's oblateness, electromagnetic forces, and solar radiation pressure. The processes act in concert so that particles paths depend on their sizes. The E ring's blue color arises because tiny particles are distributed most widely, whereas larger grains stay in the vicinity of Enceladus and probably quickly re-impact its surface. While a detailed study of R1's dynamics is beyond the scope of this paper, it seems plausible that similar processes are at work on dust in the orbit of Mab.

Mab itself was expected to fall within our October images, but no point-like feature was visible in the expected region. The 3-$\sigma$ upper limit to the disk-integrated *I/F* of any undetected satellite, derived from individual 120-s exposures, is 30 $km^2$ *(3)*. For comparison, Mab had a disk-integrated *I/F* of 50 $km^2$ in the HST data, so this body also appears to be blue.

The inner moons of Uranus are generally neutral to slightly red throughout the visual-infrared *(6,7)*. However, the five "classical" moons Miranda through Oberon turn steeply darker, by a factor of 2–3, at 2 $\mu$m, due to a strong absorption band of water ice. The inner moons show no such absorption, suggesting that water ice is absent from their surfaces. Mab orbits midway between these two populations. Because of its tiny size, Showalter and Lissauer *(1)* assumed that Mab more closely resembled the inner moons, with their very small geometric albedos of 7–10%. Our data suggest that Mab apparently has the same ice absorption band as the outer moons, indicating that it is ice-covered and therefore likely to be much brighter. With an albedo comparable to that of the outer moons (i.e., 2–4 times larger) the estimated radius of this moon drops from 12 km to 6–8 km. If this reasoning is correct, then Mab may in fact replace Cupid (~ 8 km) as Uranus's smallest regular satellite.

Keck adaptive optics images of the newly discovered outer rings of Uranus reveal a striking disparity in their colors. The outer ring, R1 (R/2003 U 1), is distinctly blue whereas the inner one, R2 (R/2003 U 2), is distinctly red. Each ring shares its color, and numerous other properties, with a similarly-located outer ring of Saturn: R1 resembles the E ring and R2 resembles the G ring. We propose that analogous dynamical processes are at work within each pair of rings. If this is correct, then R1 is likely subject to vertical perturbations comparable to its horizontal ones, so it will show a large vertical thickness when it appears edge-on to Earth in 2007. We also find that the tiny moon Mab, source of ring R1, has an icy surface more like those of the outer classical moons than of the inner family of moons. If so, then it is significantly smaller than previously estimated.

## REFERENCES AND NOTES


1. M. R. Showalter, J.J. Lissauer, *Science*, in press (2006).
2. I. de Pater, S. G. Gibbard, H. B. Hammel, *Icarus*, **180**, 186 (2006).
3. Information on materials and methods is available from *Science Online*.
4. J. A. Burns, D. P. Hamilton, M. R. Showalter, in *Interplanetary Dust*, E. Grün, B. A. S. Gustafson, S. F. Dermott, and H. Fechtig Eds. (Springer-Verlag, Berlin), 641–725 (2001).
5. R. G. French, P. D. Nicholson, C. C. Porco, E. A. Marouf, in *Uranus*, J. T. Bergstrahl, E. D. Miner, M. S. Matthews Eds. (U. Arizona Press, Tucson), 327–409 (1991).
6. E. Karkoschka, *Icarus* **151**, 51 (2001).
7. S. G. Gibbard, I. de Pater, H. B. Hammel, *Icarus* **174**, 253 (2005).
8. M. R. Showalter, J. N. Cuzzi, S. M. Larson, *Icarus* **94**, 451 (1991).
9. I. de Pater, S. C. Martin, M. R. Showalter, *Icarus* **172**, 446 (2004).
10. M. M. Hedman, *et al.*, *BAAS* **37** #66.02 (2005).
11. M. R. Showalter, J. N. Cuzzi, *Icarus* **103**, 124 (1993).
12. H. B. Throop, L. W. Esposito, *Icarus* **131**, 152 (1998).

13. T. Johnson, AGU fall meeting P21F-03 (2005).

14. M. Horanyi, J. A. Burns, D. P. Hamilton, *Icarus* **97**, 248 (1992).

15. A. Juhász, M. Horányi, *J. Geophys. Res.* **107**, 1-1 (2002).

16. This work was funded by the National Science Foundation and Technology Center for Adaptive Optics, managed by the University of California at Santa Cruz under cooperative agreement No. AST-9876783. The W.M. Keck Observatory is operated as a scientific partnership among the California Institute of Technology, the University of California and the National Aeronautics and Space Administration, and was built with financial support of the W. M. Keck Foundation. Further support was provided by NASA grants NAG5-11961 and NAG5-10451 (HBH), NNG05GL48G (MRS), and proposal numbers GO-9823, GO-10102, GO-10274, and GO-10398 from the Space Telescope Science Institute, operated by the Association of Universities for Research in Astronomy, under NASA contract NAS5-26555. SG's work was performed under the auspices of the U.S. Department of Energy, National Nuclear Security Administration by the University of California, Lawrence Livermore National Laboratory under contract No. W-7405-Eng-48.

## Supporting Online Material

www.sciencemag.org

Materials and Methods

## FIGURE LEGENDS

**Figure 1**. Keck adaptive optics images of the uranian system. (**A**) R2 is distinctly visible off the southern ansa in August, 2007; the bottom portion of this image has been enhanced relative to the planet and main rings to better show the ring. The image has been median-filtered to remove satellites. (**B**) No trace of R1 is visible at the northern ansa in October, 2007. This is a coadded mosaic, in which moving satellites appear as multiple streaks; the most prominent is Puck. Rosalind and Juliet are also visible. Horizontal white lines indicate the full radial limits of this ring.

**Figure 2**. Radial profiles through ring R2 in August (**A**) and October (**B**). Measured *I/F* is shown as dashed lines; each best-fit ring model is over-plotted in a heavy solid line. The area under this curve defines the *EW*.

**Figure 3**. Spectra of R1 (**A**) and R2 (**B**) are compared to those of Saturn's E and G rings, respectively. Measurements of Uranus's rings are shown in heavy black, Saturn's in gray. Horizontal bars indicate the range of wavelengths averaged; vertical bars indicate $\pm 1\ \sigma$. R1 is compared to a different but analogous measurement of the E ring: its peak vertically-integrated *I/F* from 1995, when the ring was viewed edge-on *(9)*; these measurements have been scaled down by a factor of 25. R2 and the G ring are both radial integrals and are plotted at the same scale.

**Figure 4**. A schematic view of the outer rings of Saturn and Uranus, in which each system has been scaled to a common planetary radius.

## SUPPORTING ONLINE MATERIALS

We observed Uranus and its ring/moon system on 23 August 2005, between 7:45 and 9:55 UT, and on 28 October 2005, between 4:50–9:10 UT, with the Keck II telescope on Mauna Kea, Hawaii. We used the adaptive optics (AO) system *(S1)* with the facility Near-Infrared Camera NIRC2, a 1024 × 1024 detector array. All observations were obtained in the K' band (1.948–2.299 μm). We used NIRC2 in high angular resolution mode, 0.00994″ ± 0.00003″ per pixel *(S2)*, which translates to 137.5 km/pixel in August, and 140.8 km/pixel in October. The ring opening angles in August and October were 8.4° and 10.5°, respectively.

All images were processed using standard near-infrared data reduction techniques (flat-fielded, sky-subtracted, with bad pixels replaced by the median of surrounding pixels). On both nights the telescope performed essentially at its diffraction limit, which is 0.046″ at K' band *(S3)*. The Strehl ratio [the ratio of the peak intensity of the observed point spread function (PSF) to the theoretical maximum for the telescope aperture] was typically between 0.5 and 0.6 both in August and in October. Using our data from July 2004 *(S2)* and the planet itself for calibration, we converted the number of counts per second into units of $I/F$, a dimensionless quantity, where $I$ is the observed intensity and $\pi F$ is the solar flux density as received by Uranus at K'.

After shifting all images to a common center, we averaged all data on 23 August and, separately, on 28 October. We used both median and regular averaging techniques. Technically, median averaging should avoid traces of satellites, but in practice this was not always the case. Hence one must be careful when searching for faint rings, since rings and satellites occupy similar regions in the uranian system.

On 23 August we combined 30 images, each with an integration time of 120 seconds, for a total integration time of one hour. In October we covered a larger field (~ 25″) by mosaicking images together. The integration time across the image is therefore not constant and some borders between frames are visible. Uranus itself and the main ring system had a total integration time of about 1.5 hours (individual images were 120 sec); the area south of the main rings a little over an hour, and the region north of the main rings 48 min.

To determine the equivalent width of a ring we followed de Pater *et al. (S2, S4)*, and determined the PSF from the ε ring, which is bright and radially unresolved. We modeled ring R2 as a uniform belt of material with a width that, after convolution with the PSF, best matched the data. In August, the best fit was obtained for a belt with a width of 1540 ± 100 km, and brightness $\mu I/F = (8.1 \pm 0.9) \times 10^{-7}$, where $\mu = \sin B = 0.146$. In October, a best fit was obtained for a belt 1270 ± 100 km wide with $\mu I/F = (1.09 \pm 0.14) \times 10^{-6}$ ($\mu$ = 0.182). The radially integrated values become $8.95 \times 10^{-6}$ in August and $9.8 \times 10^{-6}$ in October. The normal equivalent width, $\mu EW$ is obtained by multiplying these numbers with the pixel size in m, resulting in $\mu EW = 1.25 \pm 0.13$ m in August and $\mu EW = 1.39 \pm 0.22$ in October. A weighted average from the two epochs gives $\mu EW = 1.30 \pm 0.13$ m, with a radial extent of 1500 ± 100 km.

A conservative upper limit for an unresolved satellite is obtained from the RMS noise in a single 120-sec exposure, which results in a 1-σ value of $1.7 \times 10^{-5}$ (in *I/F*). We obtain the total *I/F* of a putative satellite by convolving this number with a gaussian beam with a full width at half maximum (FWHM) of 0.05″. Since a large fraction of the intensity from a satellite is lost in the PSF halo, we multiply our result by 1.49, the ratio of the total intensity to that in the core of the PSF as determined from observations of stars. Our 3-σ upper limit to the integrated *I/F* of any undetected satellite is 30 km$^2$.

We determined the upper limit to any unresolved ring in our October data as follows: We first constructed a radial profile through the expected location of ring R1 by averaging 40 columns, centered at the center of our image. The image itself is an average of the original (Fig. 1b) and vertically flipped image to increase the signal-to-noise. The RMS *I/F* noise on this profile was $7.0 \times 10^{-6}$. Since any unresolved ring would be convolved by the PSF, the radially integrated 1-σ value of a ring seen face-on becomes $\mu I/F$ is $1.4 \times 10^{-6}$. Multiplying by the pixel size in m, we obtain the equivalent width, $\mu EW$ = 0.20 m. The 3-σ upper limit to any ring with a radial extent equal to or smaller than that of the PSF would thus be 3 times this value, i.e., 0.6 m.

If the ring is broader than the PSF, the upper limit determined above is too small. HST data revealed a ring profile that is triangular in shape, peaks at 97,700 km and extends from 86,000 to 103,000 km at its base. The $\mu EW$ of such a triangular ring profile, with a peak $I/F = 7 \times 10^{-7}$, is 1 m, five times larger than the 0.2 m for an unresolved ring. Since the HST ring is ~ 10 times broader than our PSF, and triangular in shape, this number agrees with our calculations above. We scaled our modeled triangular profile up in brightness, by factors up to 3, and compared this to our data after convolution with the PSF. Since we are dealing with a broad diffuse ring, fluctuations in baseline may influence our observed profile more than the RMS noise. With this in mind, we arrive at a generous upper limit of 2.5 m to the presence of any ring resembling R1 in our data.

## REFERENCES AND NOTES


S1. P.L. Wizinowich, *et al.*, *PASP* **112**, 315 (2000).

S2. I. de Pater, S. G. Gibbard, H. B. Hammel, *Icarus*, **180**, 186 (2006).

S3. M.A. van Dam, D. Le Mignant, B.A. Macintosh, *Applied Optics* **43**, 5458 (2004).

S4. I. de Pater, *et al.*, *Icarus*, **160**, 359 (2002).

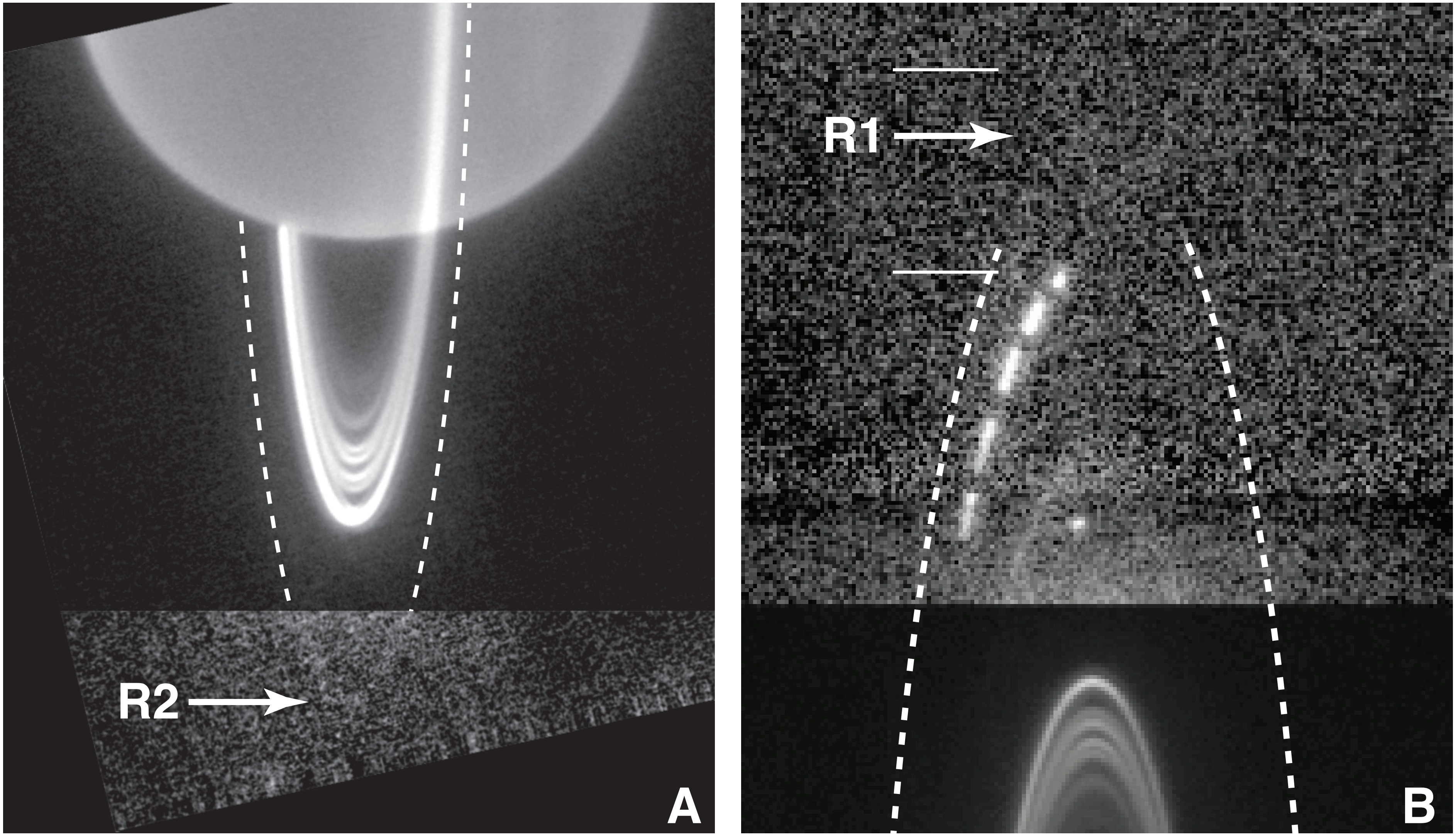
R2
A
R1
B

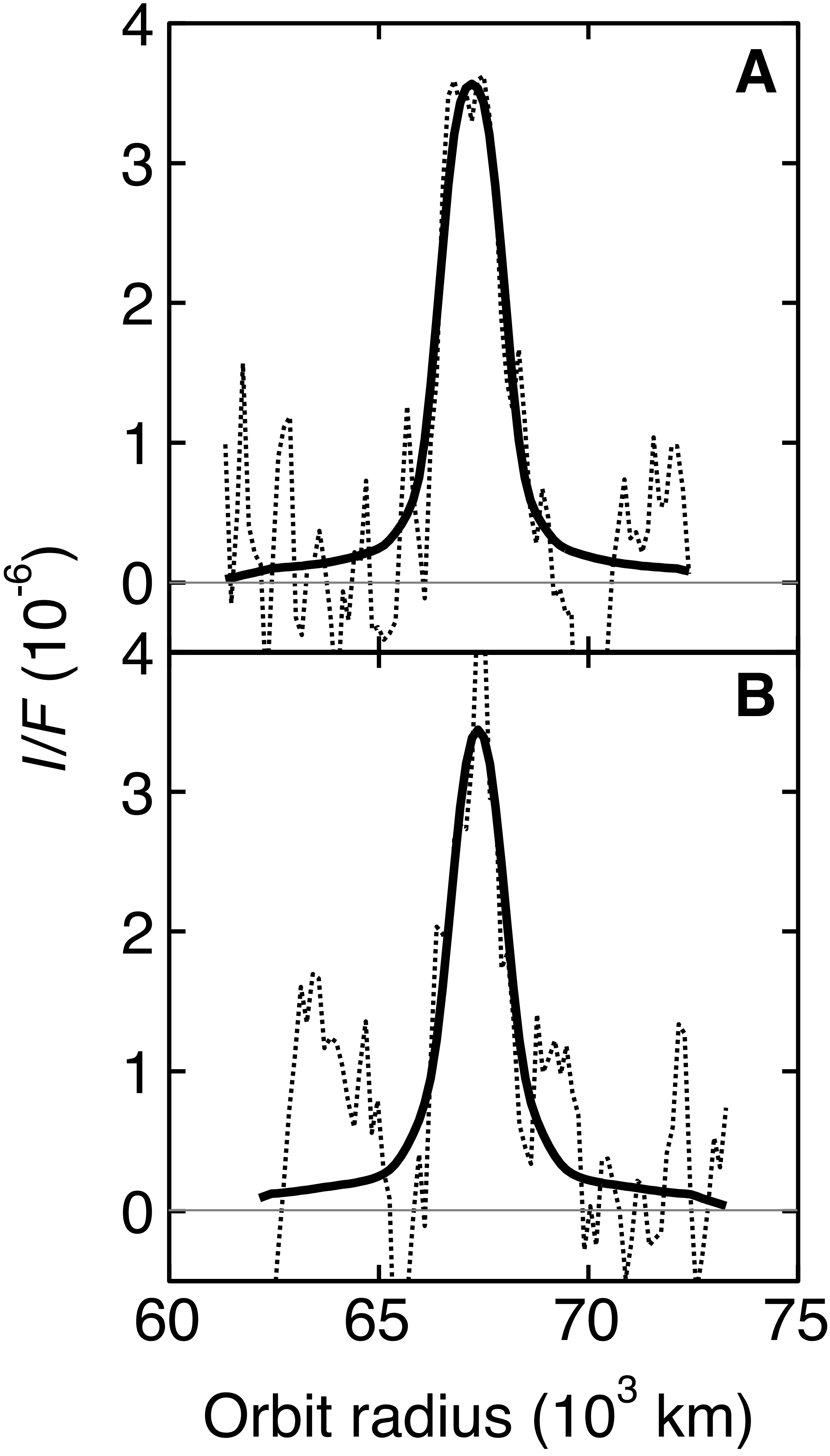


Figure 2

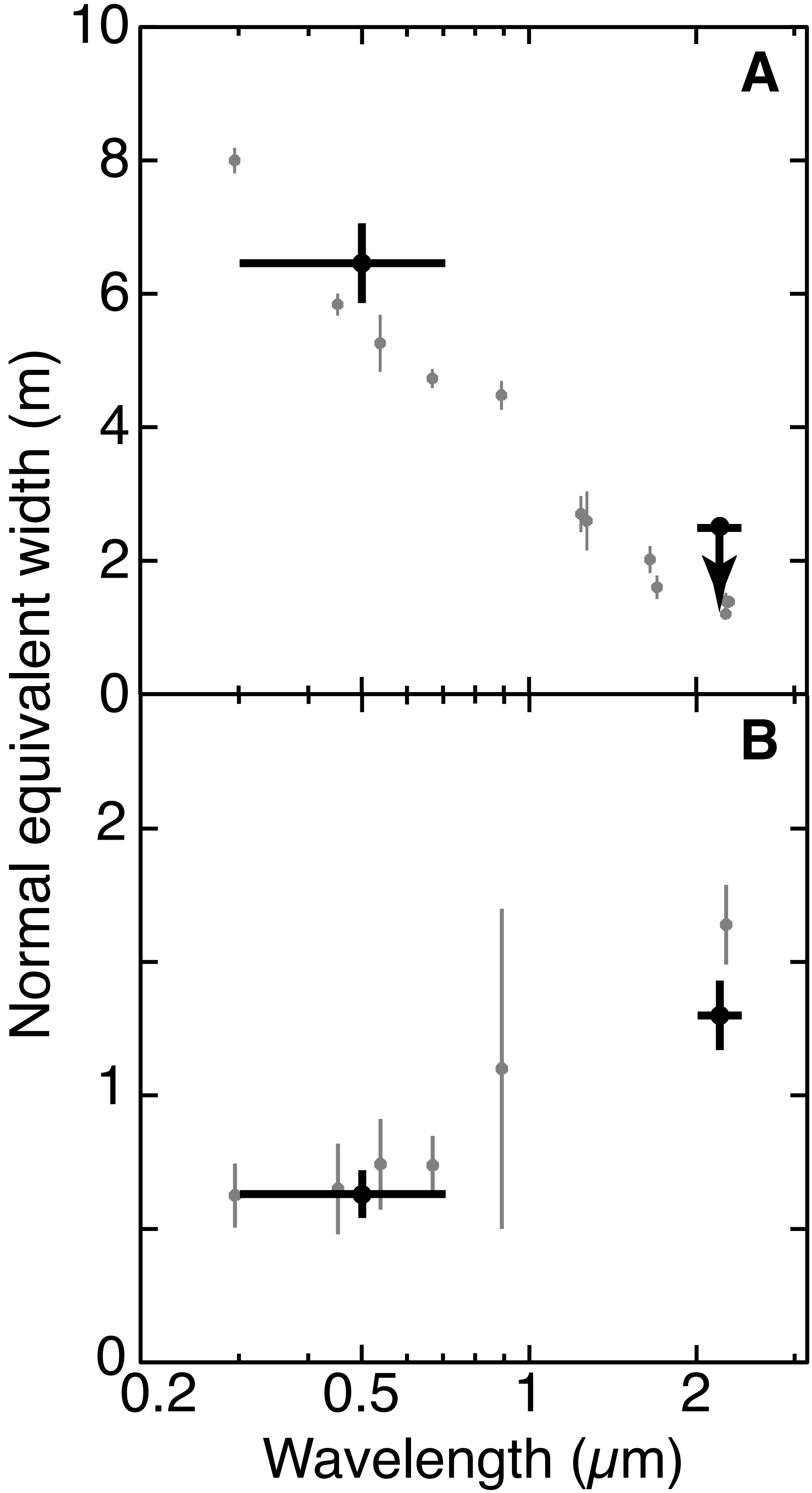
10
8
6
4
2
0
A
B
2
1
0
0.2
0.5
1
2
Normal equivalent width (m)
Wavelength (μm)

Figure 3